Macromolecules
ARTICLE

Macromolecules **2010**, *43*, 1651–1659 **1651**
DOI: 10.1021/ma902377g

A Theoretical Study of the Separation Principle in Size Exclusion Chromatography

Yanwei Wang,*,† Iwao Teraoka,‡ Flemming Y. Hansen,§ Günther H. Peters,§,⊥ and Ole Hassager†

†*Danish Polymer Center, Department of Chemical and Biochemical Engineering, Technical University of Denmark, DK-2800 Kgs. Lyngby, Denmark,* ‡*Department of Chemical and Biological Sciences, Polytechnic Institute of New York University, 333 Jay Street, Brooklyn, New York 11201,* §*Department of Chemistry, Technical University of Denmark, DK-2800 Kgs. Lyngby, Denmark, and* ⊥*MEMPHYS-Center for Biomembrane Physics*

Received October 26, 2009; Revised Manuscript Received December 8, 2009

ABSTRACT: The principle of polymer separation in size exclusion chromatography (SEC) is studied based on a classical equilibrium partitioning theory. The task is to examine the correlation between the mean span dimension of polymer chains and their equilibrium partition coefficients with confining pores. Using an extended formulation of the recently developed confinement analysis from bulk structures (CABS) method, we calculate the partition coefficients for both linear and branched polymer chains with cylindrical pores—a model pore geometry that is considered to be more realistic for voids in SEC columns than the commonly considered slit model. The partition coefficients plotted as a function of the mean span dimension relative to the pore diameter are truly universal for wide pores and nearly so for flexible polymer chains with different architectures (linear, star, two-branch-point, and comb) in the range of the partition coefficient relevant to SEC separation. We also examine the correlation between the mean span dimension and the SEC retention volume using the experimental data by Sun et al. [*Macromolecules* **2004**, *37*, 4304−4312]. It is found that when the mean span dimension is plotted as a function of the retention volume, results for both linear and branched polyethylene molecules lie nearly on the master curve determined by linear polystyrene standards. Our findings support the equilibrium thermodynamic separation principle in SEC. Since the mean span dimension is a purely geometric size parameter applicable to any chain architecture, its use in the interpretation of SEC data is appealing.

1. Introduction

Size exclusion chromatography (SEC), also referred to as gel chromatography, gel filtration, and gel permeation chromatography, as well as other names, has evolved into one of the most prevalent characterization techniques for synthetic and natural polymers, including proteins and carbon nanotubes.[1−4] However, despite a wide usage of SEC, an ambiguity about its separation principle remains unresolved.[5] It is generally believed that SEC, like other types of chromatography, is governed by equilibrium thermodynamics rather than hydrodynamics because the flow rates in the experiments generally are quite low.[6−9] On the other hand, the seminal work of Grubisic, Rempp, and Benoit[10] demonstrated that polymer molecules, regardless of chemical composition and chain architecture, separate according to the hydrodynamic volume, $V_H \propto M[\eta]$, where M is the molecular weight and $[\eta]$ the intrinsic viscosity. Since the hydrodynamic volume is a dynamic quantity, it has been puzzling for decades that a process which is believed to be an equilibrium phenomenon is controlled by a dynamic property of polymers.[5,11]

In a pioneering achievement, Casassa and co-workers developed an equilibrium theory for exclusion chromatography of branched and linear polymer chains.[12−16] The basis of their work is the idea that the separation process in SEC is determined by the equilibrium partition coefficients of solute macromolecules between a bulk dilute solution phase located at the interstitial space and confined solution phases within the pores of the column packing material.[7,17] For dilute solutions and in the absence of adsorption, the equilibrium partition coefficient (pore-to-bulk concentration ratio), K_0, is determined by the change in the configurational entropy of the polymer as it is brought into the confining geometry from the exterior bulk solution.[18,19] The number of configurations available to a polymer chain in confined spaces is less than in the bulk solution, resulting in a decrease in the configurational entropy, and thus $K_0 < 1$. Casassa and co-workers derived exact expressions for K_0 for linear and star-branched ideal polymer chains with different pore shapes including slits, cylinders, and spheres. Their calculations, subsequently verified by many experimental studies,[12,15,18,20−23] provided a solid foundation to the size-based separation principle of SEC.[1−4]

The partition coefficients generally depend on the molecular size relative to the pore size. Since there are various measures of the size of a polymer chain,[24] a fundamental problem in the theory has been the choice of a proper molecular size parameter that correlates best with K_0 for polymers of different kinds. One may think that the radius of gyration R_g is an appropriate candidate since both R_g and K_0 are equilibrium properties. However, as shown by Casassa and Tagami in 1969,[13] R_g fails to provide a universal partitioning curve for linear and star-branched polymers in a plot of K_0 vs R_g/d, where d is the pore size. For the same R_g/d value and the same pore geometry, star polymers have a smaller K_0 than linear polymers, with the most heavily branched polymers deviating the most. In an effort to

*Corresponding author. E-mail: wyw@kt.dtu.dk.

© 2010 American Chemical Society

Published on Web 01/08/2010

bring the partition curves of f-arm symmetric star polymers onto to a common curve, Casassa and Tagami proposed using $R_g g^{-1/3}$ in place of R_g. Here, g is the Zimm−Stockmayer branching parameter[25] defined as the ratio between the mean-square radius of gyration of a branched polymer and that of the linear polymer of the same molecular weight. They also showed from the Zimm−Kilb hydrodynamic theory for star-branched polymers[26] that $R_g g^{-1/3}$ is closely related to the cubic root of the hydrodynamic volume. In a recent experimental study by Sun et al.,[5] it was found that the size parameter $R_g g^{-1/3}$ for both linear and symmetric three-arm star polymers follow the same curve when plotted against the retention volume; however, the other branched types, two-branch-point and comb, failed to follow that curve. Recently, the hydrodynamic radius, R_H, has also been proposed to be used in SEC universal calibration.[27−29] For example, Teraoka[29] calculated the partition coefficients for the star, two-branch-point, and comb architectures studied in the experiments by Sun et al. for a slit confining geometry using the Green's function approach. Results of K_0 for these polymers clearly had a better correlation with R_H than with R_g.[30] Consistent with theoretical findings, Farmer et al.[31] also found in experiments that R_H correlated more satisfactorily with the retention volume than did R_g for branched polymers. In brief, the usage of $R_g g^{-1/3}$ or R_H leads to a more universal curve for the partition coefficient and to a more universal correlation with the retention volume for linear and branched polymers. This demonstrates the applicability of the classical equilibrium partitioning theory in understanding the mechanism of polymer separation in SEC. However, the use of $R_g g^{-1/3}$ or R_H in the interpretation of SEC data is obscure: it is understood that they both correlate closely with the cubic root of the hydrodynamic volume,[26,29] but it is not clearly understood why they should correlate better with polymer partitioning than does R_g, for instance.

It is known that in the limit of wide pores (K_0 near unity) the partition coefficient is a universal function of the mean span dimension of polymer chains.[23,32,33] Casassa found the universality for polymers of linear and symmetric star architectures,[13,15] and we have proven rigorously that this is in fact the case for general polymer chains regardless of details in polymer architecture and configuration statistics.[33] The physical reason for this universality is that the span dimension is determined by chain segments located at the surface of the polymer and therefore represents the relevant size of the polymer in a steric exclusion process.[7,34] This is easily seen by considering the partitioning of a uniform sphere and a spherical shell of the same diameter. The sphere and the shell are different in R_g, but obviously, they have the same mean span dimension (which is the diameter) and K_0 for a given confining geometry.

Recently, we have demonstrated the superiority of the mean span dimension over other size parameters in bringing closer the partitioning curves of linear and star-branched random walks and linear self-avoiding walks for slit, channel, and box confining geometries.[34] It is, however, considered that cylindrical pores approximate the voids in actual SEC columns most closely.[12,35] Furthermore, experimental estimates of K_0 are better fitted with Casassa's results for a cylindrical pore compared with other geometries.[18,20,21] Until now, the correlation between K_0 and the mean span dimension for cylindrical pores has not been fully analyzed. In this paper, we address this issue by developing an efficient numerical scheme for calculating K_0 for cylindrical (and spherical) pores. This is an extension of the confinement analysis from bulk structures (CABS) method developed in ref 34 for slit, channel, and box confining geometries. The new scheme allows us to systematically calculate the partition coefficients with cylindrical pores for a broad range of molecule-to-pore size ratios and for different polymer chain models including star, two-branch-point, and comb architectures as studied by Sun et al.[5] in their experiments.

This paper is organized as follows. In section 2, we briefly review the development of the mean span dimension as a useful size measure for polymer chains. In section 3, we present the CABS method for cylindrical and spherical pores. In addition, we show explicitly how the mean span dimension comes into play for wide pores. In section 4, we demonstrate the close correlation between the mean span dimension and the partition coefficients for different polymer models/architectures. In section 5, we discuss the consistency between theoretical calculations and experimental data obtained by Sun et al.[5] In particular, we give an explanation to their rather puzzling observations that the radius of gyration correlates with the partitioning of linear chains more satisfactorily than does the hydrodynamic volume whereas the reverse is true for branched chains. Finally, in section 6 we summarize our findings.

2. The Mean Span Dimension of Polymer Chains

When dealing with the diameter or width of an object, one often thinks about the distance between the teeth of a grip used to pick it up. This notion is closely related to the concept of the span dimension, X. The span dimension of a polymer chain in a given direction is defined as the shortest distance between a pair of planes normal to that direction that contain the entire chain. In other words, it is the projection length of the convex envelope of the polymer chain in that direction. The mean span dimension, $\bar{X}$, in that direction is the average over all possible orientations and conformations of the chain. In particle characterization and stereology, the mean span dimension is often called Feret's statistical diameter or the mean caliper diameter.[36,37] It is in practice a convenient measure of the particle size.

It appears that Daniels was the first to investigate the span dimension (what he termed the "extent") of a random walk.[38] A similar property was also studied by Kuhn in the context of configurational statistics of polymer chains.[39,40] Their works were later followed by those of Feller,[41] Weidmann et al.,[42] and Rubin et al.[43−49] To date, theoretical results of the span dimension have been obtained for random walk models of linear, symmetric-star, and ring polymer chains.[15,46,47] There are also Monte Carlo calculations on the span dimensions of self-avoiding walk chains.[34,44,45] Experimentally, the mean span dimension may be obtained using plane probes for micrometer-scale particles.[36,37] However, we are not aware of any measurement of the mean span dimension of polymer chains.

The orientation of a polymer chain in free solution is isotropic. Therefore, statistical properties of the span in any direction is the same as in any other directions. Suppose we view a given direction from a given point on the polymer chain. As the chain samples its orientational and conformational degrees of freedom, the maximum extent of any instant chain conformation in that direction also forms a random variable. The detailed distribution of this random variable depends on the specific choice of our observation point, but its mean value does not. Consider a given polymer conformation defined by a set of N monomer positions, $\{\mathbf{r}\} \equiv \{\mathbf{r}_1, \mathbf{r}_2, ..., \mathbf{r}_N\}$, with respect to arbitrary origin. The span dimension in a given direction, specified by unit vector $\hat{u}$, is given by (see Figure 1)

$$X = \max_i(\mathbf{r}_i \cdot \hat{u}) - \min_i(\mathbf{r}_i \cdot \hat{u}) \quad (1)$$

Here, $\max_i(\,)$ and $\min_i(\,)$ denote the maximum and minimum of the set of values of the quantity, respectively, as index i runs from 1 to N. One may also consider the span of the chain relative to a monomer position or the center of mass of the chain. The span of the chain in the $\hat{u}$ direction relative to monomer j located at $\mathbf{r}_j$ is given by

$$\beta_j = \max_i(\mathbf{r}_i \cdot \hat{u}) - \mathbf{r}_j \cdot \hat{u} \quad (2)$$

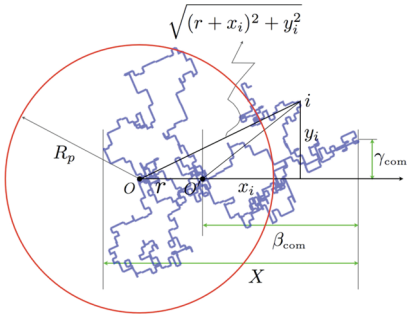

Figure 1. Cross-section view of a circular cylindrical pore of radius R_p. The circle is centered at point O. Also sketched is a static polymer conformation that is projected onto the cross-section plane with its center of mass placed at point O' at a radial position r. (x_i, y_i) denotes the relative coordinate of ith monomer to O' in an $x-y$ Cartesian coordinate system. X, β_{com}, and γ_{com} denote different distance measures that are defined in the text. The distance from the ith monomer to O is also indicated. For the given R_p and r in the figure, this conformation cannot be accommodated by the pore.

Similarly, the span of the chain in the $\hat{u}$ direction relative to the center of mass located at $\mathbf{r}_{com}$ follows

$$\beta_{com} = \max_i(\mathbf{r}_i \cdot \hat{u}) - \mathbf{r}_{com} \cdot \hat{u} \tag{3}$$

From the orientational isotropy in configuration space, it is straightforward to show that

$$\langle \beta_j \rangle = \langle \beta_{com} \rangle = \frac{1}{2}\bar{X} \tag{4}$$

holds for any given choices of j and $\hat{u}$.[33] Here, $\langle ... \rangle$ denotes an ensemble average over the orientational and conformational degrees of freedom of the polymer chain. The identity relationship given in eq 4 was used in our proof of the identity between the depletion layer thickness and one-half of the average span of a polymer chain.[33] The identity also helps us understand how the mean span dimension emerges from the CABS formulation for cylindrical pores as described in the next section.

In our earlier work presented in refs 33 and 34, symbols σ and $\langle \sigma \rangle$ were used for the span dimension and the mean span dimension. They are substituted here by X and $\bar{X}$, respectively, to be consistent with the pioneers' notation.[39,40,42] We also introduced the "steric exclusion radius" as one-half of the mean span dimension and used the symbol R_s, i.e.

$$R_s \equiv \bar{X}/2 \tag{5}$$

The same symbol is also used in the present work.

3. CABS Method for Partition Coefficients

There exist both theoretical methods and experimental techniques for studying the partitioning equilibrium of polymers between bulk and confining geometries.[18,19,32,50,51] Computer simulations have also played an indispensable role in understanding polymer partitioning in real systems. Many important factors, not accounted for in the ideal chain treatment initiated by Casassa, such as chain flexibility, excluded volume, wall adsorption, and polymer−solvent interactions, have been investigated using sophisticated simulations techniques.[52−64]

It is known that in SEC experiments the effects of solute concentration and column adsorption are suppressed.[1−4] Hence, we consider here an ideal situation of purely steric exclusion and infinitely dilute solution as studied by Casassa. Under these circumstances, the problem of finding K_0 is essentially geometrical, and the CABS method, using snapshots of polymer conformations in free space to estimate the effects of confinements, facilitates the determination of K_0 with twofold advantages: (i) compared to the rigorous analytical approach initiated by Casassa,[12] CABS is more adaptable to studies of real chain features such as a finite number of chain segments and excluded volume effects, and (ii) compared to conventional simulation approaches, CABS is superior in computational efficiency and allows us to obtain K_0 for a vast number of pore sizes solely by sampling conformations of a free chain. The formulation presented earlier in ref 34 applies only to slit, channel, and box confining geometries. Here, we extend the method to handle also circular cylinder and sphere geometries, so that all simple pore geometries that were considered by Casassa[12−16] and in many computer simulations[52−64] can be studied by CABS. For the purpose of comparison, we start by recalling the formulation for a slit geometry.

3.1. Review of the Method for a Slit Pore. Consider a slit bounded by two infinite parallel planes specified by $x = 0$ and $x = d$. Suppose that a chain is placed in the slit with its center of mass at x $(0 < x < d)$. At any x, some chain conformations will lie completely within the slit pore; others will not. Let $\rho(x)$ be the fraction of all chain conformations that lie within the pore. The equilibrium partition coefficient K_0, defined as the pore-to-bulk concentration ratio, is given by

$$K_0^{slit}(d) = \int_0^d \rho(x)\, dx / \int_0^d dx \tag{6}$$

It is easy to show that the density profile $\rho(x)$ is given by an ensemble average of the product of two Heaviside functions:[33]

$$\rho(x) = \langle H[\min_i(x + x_i)] H[d - \max_i(x + x_i)] \rangle \tag{7}$$

Here, x_i denotes the projection of the position of the ith monomer, $\mathbf{r}_i$, relative to the center of mass, $\mathbf{r}_{com}$, of the chain in the direction (let it be $\hat{u}$) normal to the slit planes, i.e.

$$x_i = (\mathbf{r}_i - \mathbf{r}_{com}) \cdot \hat{u} \tag{8}$$

Combining eqs 3 and 8, we have $\beta_{com} = \max_i(x_i)$ (see Figure 1). Substitution of eq 7 into eq 6 leads to the partition coefficient

$$K_0^{slit}(d) = \left\langle \left(1 - \frac{X}{d}\right) H\left(1 - \frac{X}{d}\right) \right\rangle \tag{9}$$

where $X = \max_i(x_i) - \min_i(x_i)$is the span dimension in the $\hat{u}$ direction as defined in eq 1. By calculating X for an ensemble of chains, K_0 can be obtained from eq 9 as a function of the slit width. Relationships analogous to eq 9 are also available for channel and box confining geometries.[34]

In the limit of wide pores ($d > X$ for all conformations), the Heaviside function in eq 9 will be equal to one, and we have

$$K_0^{slit}(d) = 1 - \bar{X}/d = 1 - \lambda, \quad \lambda \ll 1 \tag{10}$$

where $\lambda = \bar{X}/d$ is a molecule-to-pore size ratio. Equation 10 shows the universality between K_0 for a wide slit and the mean span dimension of polymer chains.[34] It is also the partition coefficient of a hard sphere of diameter $\bar{X}$ with a slit pore of width $d \geq \bar{X}$.

3.2. Extension to Cylindrical and Spherical Pores. Consider a polymer chain that is placed with its center of mass, denoted by point O', at a radial position r within a circular cylinder of radius R_p as shown in Figure 1. The length of the cylinder is considered to be infinite so that we neglect end

effects. We define a slicing plane through O' and perpendicular to the cylinder axis which intersects the plane at point O. In that plane, we set up an $x-y$ Cartesian coordinate system with origin at O' and with the x-axis along the line connecting O and O'. The polymer chain consists of a number of monomers. A chain conformation lies completely within the pore if the maximum distance from point O to all the monomers is less than R_p. Thus, we may write the fraction of all chain conformations that lie within the pore, $\rho(r)$, in the form analogous to eq 7

$$\rho(r) = \langle H[R_p - \max_i(\sqrt{(r+x_i)^2 + y_i^2})]\rangle \quad (11)$$

where (x_i, y_i) denotes the position of the ith monomer relative to the center of mass O' in the aforesaid coordinate system.

For a given chain conformation, the Heaviside function in the above equation is equal to one only if

$$r^2 + 2x_i r + x_i^2 + y_i^2 - R_p^2 < 0 \qquad \text{for all } i = 1, 2, ..., N \quad (12)$$

By finding the range of r in which the above condition holds, we may rewrite eq 11 as

$$\rho(r) = \langle H(r - r_-)H(r_+ - r)H(r_+ - r_-)H(R_p^2 - y_i^2)\rangle \quad (13)$$

where the two end points, r_- and r_+, are given by

$$r_- = \max_i(0, -x_i - \sqrt{R_p^2 - y_i^2}) \quad (14)$$

$$r_+ = \min_i(-x_i + \sqrt{R_p^2 - y_i^2}) \quad (15)$$

Similar to eq 6, the partition coefficient for a circular cylinder is given by

$$K_0^{\text{cylinder}}(R_p) = \int_0^{R_p} \rho(r) r\, dr \Big/ \int_0^{R_p} r\, dr \quad (16)$$

Substitution of eq 13 into eq 16 leads to

$$K_0^{\text{cylinder}}(R_p) = \left\langle \frac{1}{R_p^2}(r_+^2 - r_-^2)H(r_+ - r_-)H(R_p^2 - y_i^2)\right\rangle \quad (17)$$

This may be used to determine the partition coefficients for any pore size R_p by sampling a given set of polymer configurations in bulk.

It is straightforward to extend the above treatment for a cylinder to a spherical cavity. Analogous to eq 17, the CABS formulation of K_0 for a spherical pore of radius R_p is found to be

$$K_0^{\text{sphere}}(R_p) = \left\langle \frac{1}{R_p^3}(r_+^3 - r_-^3)H(r_+ - r_-)H(R_p^2 - y_i^2 - z_i^2)\right\rangle \quad (18)$$

with r_+ and r_- now given by

$$r_- = \max[0, \max_i(-x_i - \sqrt{R_p^2 - y_i^2 - z_i^2})] \quad (19)$$

$$r_+ = \min_i(-x_i + \sqrt{R_p^2 - y_i^2 - z_i^2}) \quad (20)$$

Here, (x_i, y_i, z_i) denotes the position of the ith monomer relative to the center of mass O'.

It is interesting to examine eq 17 for a wide cylindrical pore. Consider a situation in which $R_p^2 > x_i^2 + y_i^2$ holds for all i and for all chain conformations such that $r_- = 0$, $r_+ > r_-$, and $R_p^2 > y_i^2$. Equation 17 thus reduces to

$$K_0^{\text{cylinder}}(R_p) = \langle r_+^2/R_p^2\rangle = \left\langle \min_i\left[1 - 2\frac{x_i}{R_s}\lambda + \frac{x_i^2 - y_i^2}{R_s^2}\lambda^2 + \mathcal{O}(\lambda^3)\right]\right\rangle \quad (21)$$

where $\lambda = R_s/R_p = \bar{X}/d$ with $d = 2R_p$ being the pore diameter. Since we consider wide pores where $\lambda \ll 1$, the function inside the ensemble average in eq 21 takes its minimum value when x_i takes its maximum, $\beta_{\text{com}} = \max_i(x_i)$ as introduced earlier. Substitution of β_{com} for x_i in eq 21 leads to

$$K_0^{\text{cylinder}}(\lambda) = 1 - 2\lambda + C_2\lambda^2 + \mathcal{O}(\lambda^3) \quad (22)$$

which shows the universality between the partition coefficient and the mean span dimension of polymer chains in the case of $\lambda \ll 1$. Compared to the result for a slit in eq 10, the fact of 2 in the linear term is due to the two-dimensional confinement effect in the case of a cylindrical pore. The quantity C_2 in eq 22 is characteristic to the shape (roundness) of the outer surface of the molecule and is defined by

$$C_2 = (\langle\beta_{\text{com}}^2\rangle - \langle\gamma_{\text{com}}^2\rangle)/R_s^2 \quad (23)$$

where $\gamma_{\text{com}} = y_k$ with the monomer index k being determined from equation $x_k = \max_i(x_i)$ (see Figure 1). It is found that C_2 is 0 for a thin rod and 1 for a sphere.[65] The primary goal of introducing the C_2 parameter is to quantify the onset of departure from universality, as is discussed in section 4.

3.3. Numerical Implementation and Validation. Numerical implementations of eqs 17 and 18 are simple and straightforward, as it was the case with slit, channel, and box confining geometries.[34] In fact, it is possible to make a program that, every time a new polymer conformation is generated, calculates contributions to various size parameters (such as $\bar{X}$, R_g, and R_H) as well as K_0 for different confining geometries. $\bar{X}$ may be obtained by an ensemble average of X given by eq 1. R_g and R_H are calculated from their monomer positions (eqs 1 and 2 in ref 29). K_0 for various pore geometries are obtained using the CABS method, i.e., eq 17 for cylinders, eq 18 for spheres, and eqs 23−25 in ref 34 for slits, channels, and boxes, respectively. The total number of polymer conformations used in our calculations ranged from 10^5 to 10^6. For calculating K_0 and $\bar{X}$, we used 10 sets of orthonormal vectors of isotropic orientations for each conformation to improve the sampling efficiency.[33,34]

To demonstrate the accuracy of our calculations of K_0 with the CABS method, we have compared our results with scaling predictions[32,50,66−70] for both random walk (RW) and self-avoiding walk (SAW) chains. In our simulations, RW chains were sampled by performing simple random walks in continuous space, and SAW chains were sampled on simple cubic lattices using the pivot algorithm.[71] Our results, included in the Supporting Information, are consistent with the scaling-law predictions for both RW and SAW and for various confining geometries. Furthermore, we have also compared our results with some prior simulations results in the literature. In particular, the CABS method

for cylindrical pores, eq 17, was applied to calculate the partition coefficients of (i) linear RW chains of different number of steps as studied by Davidson et al.[53] and (ii) linear wormlike chains of different ratios of persistence length to contour length as studied by Teraoka et al.[18,72] In both cases, our results (not shown) are in good agreement with their reported data.

It should be noted that the CABS method in principle applies to both wide and narrow pores; however, for very narrow pores relative to the size of the polymer in bulk, the CABS method for determining K_0 becomes very inefficient. This is because the equilibrium conformations of a polymer chain in the highly confined state are very different from those in free space, and nearly all polymer conformations sampled from bulk will not fit into the pore. It is therefore necessary to sample a huge number of conformations to obtain a good statistics for $K_0 < 10^{-7}$. This drawback may be overcome by employing configurational bias techniques. However, since in SEC the elution volume is a linear function of K_0, such small K_0 values are not relevant to the SEC separation. They all correspond to the exclusion limit.[19]

4. K_0 as a Function of the Mean Span Dimension

The correlation between K_0 and $\bar{X}$ for many different model polymers is examined in this section. We show here plots of K_0 as a function of R_s/R_p ($= \bar{X}/d$) for cylindrical pores only. Plots of K_0 as a function of R_g/R_p, $R_g g^{-1/3}/R_p$, and R_H/R_p for cylindrical pores as well as spherical cavities are available in the Supporting Information. They provide additional evidence of the superiority of $\bar{X}$ in correlation with K_0 over the other size parameters.

We have considered three groups of nearly monodisperse polymers studied by Sun et al.[5] in their experiments. The three groups are (i) linear polystyrene with molecular weight M ranging from 9800 to 2.6×10^6 g/mol, (ii) linear polyethylene with M ranging from 6600 to 8.3×10^5 g/mol, and (iii) 37 branched polyethylenes including 3-arm star (both symmetric and asymmetric), two-branch-point, and comb architectures. Details of their experimental data can be found in Tables 2−6 in ref 5. Our calculations employed a simple discrete RW model in continuous space for each of their sample molecules. For the branched samples, each primary chain was generated as a RW trajectory with the connectivity of the primary chains resembling the large-scale chain architecture of the real molecule. The number of mass points (i.e., the number of steps + 1) in each of our model chains was obtained from the reported molecular weight data (measured data for linear samples and target data for branched ones) in ref 5 and the molar mass of Kuhn segments, M_0, which is 720 g/mol for polystyrene and 150 g/mol for polyethylene.[73] Details of our model chains are given in the Supporting Information. For convenience, the same sample designation as used by Sun et al. is followed. For example, consider PEH$(10)_2(95)(10)_2$ which is a branched polyethylene sample having a two-branch-point structure with two arms per branch point. On the basis of the target molecular weights (available in Table 4 in ref 5) for each arm and the connector and the M_0 value for polyethylene, we used 68 mass points for each arm and 662 mass points for the connector for our RW model chain.

Figure 2 shows our CABS results for various different flexible polymers including the 37 different branched polymers with different architectures (star, two-branch-point, and comb), linear RW polymers with mass points ranging from 15 to 5000 (the effect of finite number of mass points is further investigated). The results, grouped as flexible polymers in Figure 2, also include theoretical results for ideal chains of linear and symmetric star (with 3, 4, up to 12 arms) architectures based on the analytical

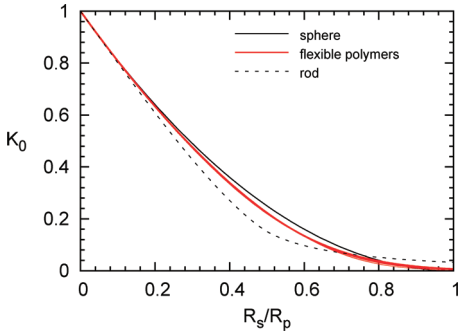

Figure 2. K_0 as a function of R_s/R_p for a large number of different (linear and branched, RW and SAW) flexible polymers and cylindrical pores. Details are given in the text. For comparison, results for a sphere and a rod are also shown.

expressions by Casassa and Tagami.[13] To the best of our knowledge, this is the first time a plot of K_0 for cylindrical pores versus the span dimension is presented. It demonstrates that the partitioning curves for different flexible polymers are truly universal in the permeation limit (where K_0 near unity) as shown in eq 22 and nearly so over the entire range of K_0 relevant to SEC separation. This is, however, not the case if K_0 is plotted versus some of the other size parameters (R_g, $R_g g^{-1/3}$, R_H) as demonstrated in the Supporting Information. There, the superiority of the span dimension is also shown for spherical pores.

It should be noted that SEC experiments are typically conducted under good solvent conditions, and thus it would have been more appropriate to use the SAW model that takes into account excluded volume interactions. We employed the RW model because of its simplicity, and in addition, utility of studying the partitioning of RW chains has also been demonstrated by the convincing achievements of Casassa's approach based on ideal chain statistics.[29] However, to assess the effect of excluded volume interactions, we also included in the group of flexible polymers in Figure 2 a linear SAW chain of 10^3 steps, and as shown, its partitioning curve coincides with those of RW chains. This indicates that the universality is not influenced by excluded volume interactions in the range of K_0 relevant to SEC separation, although the actual values of R_s and thus K_0 for a given pore size certainly depend on the solvent conditions.[34]

Figure 2 also includes a comparison of the partitioning curves of flexible polymers to those of a sphere and a rod. For a sphere of radius R_s, K_0 for a cylindrical pore of radius R_p is $K_0 = (1 - R_s/R_p)^2$ for $R_s \le R_p$ and is zero otherwise. This is the same as that for a square channel of width $d = 2R_p$. For a rod molecule of length L (and $R_s = L/4$) and a cylindrical pore, K_0 was given by Giddings et al. in terms of elliptic integrals,[7] which also coincides with our numerical results obtained from eq 17. Figure 2 shows that sphere and rod do not fall onto the results for flexible polymers except in the permeation limit. At $R_s/R_p = 0.4$ for example, a sphere has the largest K_0 and a rod the least. In contrast, for large R_s/R_p values, e.g., at $R_s/R_p = 1$, the order is reversed. In an experimental study by Dubin and Principe,[74] a failure of the V_H-based universal calibration approach for rodlike macromolecules versus random coils and globular proteins was found, and they also considered other size parameters including the mean span dimensions which were estimated from the hydrodynamic volume data based on expressions given by Casassa.[15] They demonstrated (in Figure 5 in ref 74) that $\bar{X}$ failed to unify the elution behavior of their samples. In their experiments, K_0 spans approximately from 0.1 to 0.8, and our theoretical results in Figure 2 do not show a universal partitioning behavior, either. In addition, a crossover in K_0 between the rigid rod and flexible coils was observed in their results at large $\bar{X}$ values, in agreement with our findings. However, the large difference between flexible coil

and globular proteins in their results cannot be explained by Figure 2. A switch from the cylinder pore model to other pore geometries does not explain the discrepancy, either.

To have a better understanding of the difference in the partition coefficients for a rod, flexible polymer chains, and a sphere, we also investigated the partitioning of spheroids, worm-like chains, and simple RW chains with only a few steps into cylindrical pores. Results are presented in the Supporting Information. One may summarize them by identifying four ranges of R_s/R_p. In the limit of wide pores ($R_s/R_p \to 0$), all partition curves collapse onto a single curve. In the range of $0.1 \le R_s/R_p \le 0.6$, K_0 for the same R_s/R_p value is sorted by the roundness parameter C_2 calculated using eq 23. In contrast, for very large values of R_s/R_p, the order of K_0 is determined by the ability of a molecule to enter a narrow pore by adjusting its orientation or internal conformations. Between these two ranges, the partition curves intersect each other. Although in those cases K_0 as a function of R_s/R_p does not follow a unique curve, the disparity between different partition curves is significantly less than that found when other size parameters (R_g for instance) are used.

5. Comparison with Experiments

We have demonstrated that the theoretical partition curves of flexible polymers follow a nearly universal curve in the plot of K_0 as a function of R_s/R_p in the range of K_0 relevant to SEC separation. It is thus interesting to examine how good this universality is in experiments.

We consider the experimental data obtained by Sun et al.[5] and estimate R_s of their polymer samples using their R_g data and values of R_s/R_g obtained from our calculations. Two approaches were used to calculate R_s/R_g: one from simulations of finite RW chains and the other from the continuum limit (ideal chains). As we noted earlier, it is straightforward to calculate various bulk size parameters including R_s, R_g, and R_H as well as their ratios from simulations. On the other hand, it is perhaps more of theoretical interest to be able to determine those size parameters from the continuum limit. For ideal chains having the branched architectures studied by Sun et al., results of R_g and R_H are available in the work by Teraoka,[29] and results of R_s are obtained here using an approach described in the Appendix. Results from both approaches are consistent with each other. These data are listed in Tables 1−4 in the Supporting Information. Note that because of the difference between discrete and continuum models, the results of R_s/R_g from simulations are smaller by 2−3% (except for the linear RW chains of only a few steps) compared with those for the continuum limit; in contrast, the results of R_H/R_g from simulations are slightly larger than those for the continuum limit.[34,75]

Figure 3 demonstrates the correlation between the span dimension and the experimental SEC retention volume on a semilog plot of R_s^3 vs retention volume. Results of R_s/R_g obtained from the continuum limit are used, but the positions of the symbols hardly change if simulation results of R_s/R_g are used instead. Different symbols in Figure 3 denote different categories of model polymers. Both the linear and branched polyethylenes lie closely to the curve determined for the linear polystyrene standards. For the linear and branched polyethylene samples, Figure 3 shows that R_s^3 correlates better with the retention volume than does R_g^3 (see Figure 6a in ref 5). The universality of the curve is comparable to those using $[\eta]M$ (see Figure 6b in ref 5) and R_H^3 (Figure 6b in ref 29). It is difficult to judge which one correlates best with SEC separation since they all provide intimate correlations with the retention volume. However, Figure 3 also shows that linear polyethylene follows the common R_s^3 curve over the entire range of sizes, in the same way as the common R_g^3 curve obtained by Sun et al. in Figure 5a in ref 5,

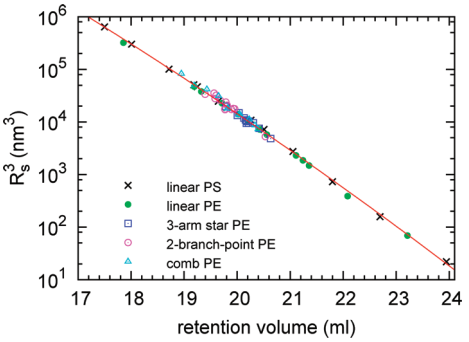

Figure 3. Semilog plot of R_s^3 versus retention volume for linear polystyrene (PS) standards and linear and branched polyethylene (PE) molecules. R_s is estimated from experimental data of R_g and the characteristic ratio R_s/R_g obtained from the continuum limit. The original data of R_g and retention volumes are obtained by Sun et al.[5] The solid line is a fit to the polystyrene data.

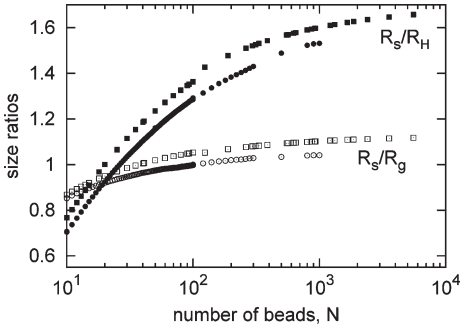

Figure 4. Characteristic size ratios, R_s/R_g (open symbols) and R_s/R_H (closed symbols), are shown as a function of the total number of mass points, N, for linear RW (square) and SAW (circle) chains.

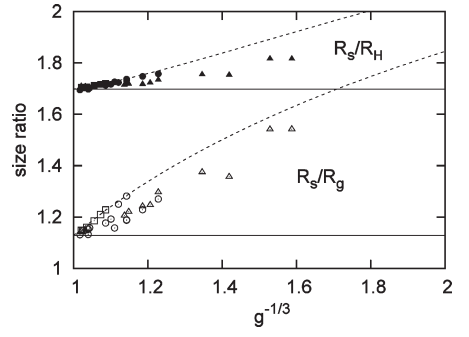

Figure 5. Characteristic size ratios, R_s/R_g (open symbols) and R_s/R_H (closed symbols), shown as a function of $g^{-1/3}$ for branched polymers. The symbols represent 3-arm stars (square), 2-branch-point (circle), and comb (triangle) architectures. The dashed lines are for f-arm symmetric star polymers with $g = (3f - 2)/f^2$, $R_s/R_g = (2/\sqrt{\pi})(g_s/g)^{1/2}$, and $R_s/R_H = [16/(3\pi)](g_s/g_H)^{1/2}$ where $g_s = f^{1/2}\int_0^\infty[\mathrm{erf}(t^{1/2})]^{f-1}\exp(-t)\,dt$ and $g_H = f[(\sqrt{2} - 1)(\sqrt{2} + f)]^2$. The left ends of the dashed lines correspond to a linear ideal chain with $g = 1$, $R_s/R_g = 2/\sqrt{\pi}$, and $R_s/R_H = 16/(3\pi)$. The solid horizontal lines, shown to guide the eye, correspond to the results for a linear ideal chain.

and in this case, when $[\eta]M$ was used in place of R_g^3, the agreement between the series was not as good, especially in the low end of the molecular weight range.[5]

Note that we have not taken into account the effect of excluded volume interactions to R_s/R_g for our estimations of R_s in Figure 3. Simulation results demonstrate that the R_s/R_g value of a linear RW chain is slightly larger than that of a linear SAW chain of the same total number of mass points, N (see Figure 4 and also Figure 3 in ref 34). Consider, for instance, $N = 10^3$: we obtained $R_s/R_g = 1.1049$ for RW and $R_s/R_g = 1.0405$ for SAW.

This indicates that our estimations of R_s based on RW data may overestimate the actual value by about 6%. If this difference holds for both linear and branched chains, the universality shown in Figure 3 will not be affected. However, previous studies on the branching parameter, g, revealed that g values in good solvents are in rather good agreement with those from ideal chain calculations for stars, but noticeable deviations are found for other branched structures, especially when composed of many long branches.[76,77] Similarly, the effect of excluded volume interactions may also have different impacts on R_s/R_g values for different chain architectures. Therefore, it would be interesting to examine the correlation between R_s and retention volume using R_s/R_g data obtained from SAW simulations. We expect this would further improve the universality shown in Figure 3.

Sun et al. concluded from their experiments that R_g of linear chains correlates better with the SEC retention volumes than does the hydrodynamic volume whereas the reverse is the case for branched chains. To the best of our knowledge, this somewhat puzzling conclusion has not been explained, and in the following, we seek to address this issue based on our calculations. We did not calculate the hydrodynamic volume because of known difficulties,[29] and therefore we rely on the experimental findings that the ratio $[\eta]M/R_H^3$ varies little for polymers of different molecular weights and chain architectures.[78]

Figure 4 shows simulation results of R_s/R_g (open symbols) and R_s/R_H (closed symbols) as a function of the total number of mass points N, for linear RW (square) and SAW (circle) chains. As discussed earlier, there is a difference between RW and SAW chains. However, for both types of chains, the ratios increase with N to their limiting values as $N \rightarrow +\infty$ with a slope that is smaller for the R_s/R_g curve than for the R_s/R_H curve. This implies that if two linear polymers of different length (N) have the same R_s and therefore the same retention volume in SEC experiments, then the difference in the R_g values for the two polymers will be smaller than the difference in their R_H values. This explains why for linear chains R_g correlates better with the SEC retention volumes than does the hydrodynamic radius (and the hydrodynamic volume) as was found by Sun et al. in their experiments.[5] Furthermore, Figure 4 also explains why at low molecular weights linear polystyrene has a larger hydrodynamic volume than does linear polyethylene of the same retention volume. Recall that the Kuhn length value is 1.8 nm for polystyrene and 1.4 nm for polyethylene,[73] and therefore for the same R_s (and consequently the same retention volume), linear polystyrene will have fewer total number of beads than linear polyethylene and therefore a larger hydrodynamic radius (hydrodynamic volume).

Figure 5 shows the effect of long chain branching on the size ratios, R_s/R_g and R_s/R_H, for the model branched chains of star, 2-branch-point, and comb architectures. All size parameters are obtained from the continuum limit. The abscissa, $g^{-1/3}$, increases with an increase of long chain branching. Both ratios are larger for branched chains than for a linear chain.[79] This implies that if a branched chain and a linear chain have the same R_g, then the branched chain will have a larger mean span dimension and thus elute earlier in SEC experiments. This is consistent with the findings by Sun et al. (Figure 6a in ref 5) and Farmer et al. (Figures 8 and 10 in ref 31). However, contrary to the case in Figure 4, Figure 5 shows that R_s/R_H changes less with an change in $g^{-1/3}$ than does R_s/R_g. This implies that if two polymers of different branching parameters have the same R_s and therefore the same retention volume, then the difference in their R_H values will be smaller than the difference in their R_g values. This explains why for branched chains the calibration curve using R_H or V_H is superior to the one using R_g, as was also found by Sun et al.[5] and Farmer et al.[31] in their experimental studies.

6. Concluding Remarks

The CABS method allows efficient computation of the equilibrium partition coefficients K_0 for various model polymer chains and a large number of different pore sizes. In this work, we extended the CABS method to cylindrical and spherical pores, and thereby all simple model pore geometries that are usually considered in theory and simulation studies can now be studied by CABS.

We have demonstrated that results of K_0 plotted as a function of $\bar{X}/d$ ($= R_s/R_p$) nearly overlap for the several flexible polymer chains including linear, star, two-branch-point, and comb architectures in the range of the partition coefficient relevant to SEC separation. A comparison of the universality of K_0 with other size parameters, such as the radius of gyration and the hydrodynamic radius, also demonstrates that the mean span dimension is more relevant to confinement effects.

The intimate correlation between $\bar{X}$ and K_0 for flexible polymers was also demonstrated using the experimental data obtained by Sun et al. in their study of SEC separation. In a plot of R_s vs retention volume, we found that both their linear and branched polyethylene molecules lie nearly on the curve determined by the linear polystyrene standards. Furthermore, we also provide an explanation to their rather puzzling experimental findings by examining the effects of finite number of chain segments and long chain branching on the characteristic size ratios, R_s/R_g and R_s/R_H.

The consistency between the equilibrium partitioning theory and the experimental findings by Sun et al. demonstrates applicability of the theory to SEC separation. Since the mean span dimension is a purely geometric size parameter applicable to any chain architecture, its use in the interpretation of SEC data is appealing. One may in fact regard SEC as a method to probe the mean span dimension for each fraction in an SEC chromatogram. This may help infer the branching architecture of a given polymer chain from its retention volume. Furthermore, since the mean span dimension can be calculated for various types of chain architectures, it may be applied to simulations of SEC elution curves on the basis of polymerization kinetics (such as the method developed by Tobita and co-workers).[80−82]

Acknowledgment. Stimulating discussions with J. J. de Pablo and A. Shapiro are gratefully acknowledged. Y.W. acknowledges financial support by the Danish Research Council for Technology and Production Sciences under Grant 274-08-0051. G.H.P. acknowledges financial support from the Danish National Research Foundation via a grant to MEMPHYS-Center for Biomembrane Physics. Simulations were performed at the Danish Center for Scientific Computing at the Technical University of Denmark.

Appendix: Calculations for the Mean Span Dimension of Ideal Chains

Assuming ideal chain statistics, formulas for the mean-square radius of gyration and the hydrodynamic radius of various branched polymer molecules have been obtained since the pioneering work of Zimm and Stockmayer.[25,29] In contrast, results available for the mean span dimension, $\bar{X}$, of branched chains are scarce. It is thus desirable to formulate a systematic approach to obtain $\bar{X}$ for various branched architectures. This is achieved in the following way.

First we remark that, in the weak confinement limit, K_0 is a universal function of the mean span dimension.[33,34] For a slit confining geometry of width d, this is given by eq 10. Solving eq 10 for $\bar{X}$ gives

$$\bar{X}/R_g = \lim_{R_g/d \rightarrow 0} \frac{1 - K_0^{slit}(R_g/d)}{R_g/d} \qquad (24)$$

where the radius of gyration R_g is used as a length scale factor. Second, we note that Teraoka has obtained expressions of K_0 for the slit geometry for branched ideal chains of asymmetric star, 2-branch-point, and comb architectures using the Green's function approach (which is in principle applicable to other branched types).[29] Unfortunately, inserting those expressions of K_0^{slit} into eq 24 generally does not yield $\bar{X}$ in terms of elementary functions for branched chains. Numerical calculations are necessary, even for symmetric star polymers. However, for practical purposes, it is sufficient to approximate the limit in eq 24 as R_g/d approaches zero by letting $R_g/d = 0.1$. Thereby, we have

$$\bar{X}/R_g \approx 10[1 - K_0^{slit}(R_g/d = 0.1)] \quad (25)$$

This makes it friendly for numerical calculations. We have examined the validity of eq 25 for all our calculations. Consider e.g. a linear chain: truncating the infinite summation in Casassa's expression (eq 4 in ref 12) at $m = 10$; eq 25 gives an estimation of $\bar{X}/R_g$ that is accurate down to the 11th digit compared to the exact result, $4/\sqrt{\pi}$.[34]

Supporting Information Available: Comparison of our results of K_0 with scaling-law predictions to demonstrate the accuracy of CABS calculations; plots similar to Figure 2 but with R_s substituted by other parameters (R_g, $R_g g^{-1/3}$, and R_H), as well as results for a spherical cavity to further demonstrate the superiority of the mean span dimension in collapsing the partitioning curves of flexible polymers to a single curve; results of the partitioning of spheroids, wormlike chains, and RW chains with only a few steps into cylindrical pores to demonstrate the transition in Figure 2 in the partitioning behavior from a rod to flexible polymer chains and to a sphere; and tabulation of calculation results of R_s/R_g and R_H/R_g obtained from simulations and from the continuum limit for the polymer samples studied by Sun et al. in their experiments. This material is available free of charge via the Internet at http://pubs.acs.org.

References and Notes

(1) Yau, W. W.; Kirkland, J. J.; Bly, D. D. *Modern Size Exclusion Chromatography*; Wiley-Interscience: New York, 1979.
(2) Glöckner, G. *Polymer Characterization by Liquid Chromatography*; Elsevier: New York, 1987.
(3) Mori, S.; Barth, H. G. *Size Exclusion Chromatography*; Springer: Berlin, 1999.
(4) *Handbook of Size Exclusion Chromatography and Related Techniques*, 2nd ed.; Wu, C.-S., Ed.; Marcel Dekker: New York, 2004.
(5) Sun, T.; Chance, R. R.; Graessley, W. W.; Lohse, D. J. *Macromolecules* **2004**, *37*, 4304–4312.
(6) Moore, J. C. *J. Polym. Sci., Part A* **1964**, *2*, 835–843.
(7) Giddings, J. C.; Kucera, E.; Russell, C. P.; Myers, M. N. *J. Phys. Chem.* **1968**, *72*, 4397–4408.
(8) Klein, J.; Grüneberg, M. *Macromolecules* **1981**, *14*, 1411–1415.
(9) Giddings, J. C. *Unified Separation Science*; Wiley-Interscience: New York, 1991.
(10) Grubisic, Z.; Rempp, P.; Benoit, H. *J. Polym. Sci., Polym. Lett.* **1967**, *5*, 753–759.
(11) des Cloizeaux, J.; Jannink, G. *Polymers in Solution: Their Modelling and Structure*; Clarendon: Oxford, 1990.
(12) Casassa, E. F. *J. Polym. Sci., Polym. Lett.* **1967**, *5*, 773–778.
(13) Casassa, E. F.; Tagami, Y. *Macromolecules* **1969**, *2*, 14–26.
(14) Casassa, E. F. *J. Phys. Chem.* **1971**, *75*, 3929–3939.
(15) Casassa, E. F. *Macromolecules* **1976**, *9*, 182–185.
(16) Casassa, E. F. *J. Polym. Sci., Polym. Symp.* **1985**, *72*, 151–160.
(17) Laurent, T. C.; Killander, J. *J. Chromatogr.* **1964**, *14*, 317–330.
(18) Teraoka, I. *Prog. Polym. Sci.* **1996**, *21*, 89–149.
(19) Teraoka, I. *Polymer Solutions: An Introduction to Physical Properties*; John Wiley & Sons: New York, 2002.
(20) Yau, W. W.; Malone, C. P. *Polym. Prepr.* **1971**, *12*, 797–803.
(21) Satterfield, C. N.; Colton, C. K.; de Turckheim, B.; Copeland, T. M. *AIChE J.* **1978**, *24*, 937–940.
(22) Haller, W. *Macromolecules* **1977**, *10*, 83–86.
(23) Gorbunov, A. A.; Solovyova, L. Y.; Pasechnik, V. A. *J. Chromatogr., A* **1988**, *448*, 307–332.
(24) Volkenstein, M. V. *Configuration Statistics of Polymer Chains*; Interscience: New York, 1963.
(25) Zimm, B. H.; Stockmayer, W. H. *J. Chem. Phys.* **1949**, *17*, 1301–1314.
(26) Zimm, B. H.; Kilb, R. W. *J. Polym. Sci.* **1959**, *37*, 19–42.
(27) Radke, W. *Macromol. Theory Simul.* **2001**, *10*, 668–675.
(28) Radke, W. *J. Chromatogr., A* **2004**, *1028*, 211–218.
(29) Teraoka, I. *Macromolecules* **2004**, *37*, 6632–6639.
(30) Assuming the Oseen tensor for the hydrodynamic interaction between the beads in the molecule (Kirkwood approximation), R_H was estimated as the reciprocal of the mean of the reciprocal distance between a pair of segments for equilibrium conformation.
(31) Farmer, B. S.; Terao, K.; Mays, J. W. *Int. J. Polym. Anal. Charact.* **2006**, *11*, 3–19.
(32) Gorbunov, A. A.; Skvortsov, A. M. *Adv. Colloid Interface Sci.* **1995**, *62*, 31–108.
(33) Wang, Y.; Hansen, F. Y.; Peters, G. H.; Hassager, O. *J. Chem. Phys.* **2008**, *129*, 074904.
(34) Wang, Y.; Peters, G. H.; Hansen, F. Y.; Hassager, O. *J. Chem. Phys.* **2008**, *128*, 124904.
(35) Knox, J. H.; Scott, H. P. *J. Chromatogr., A* **1984**, *316*, 311–332.
(36) Walton, W. H. *Nature* **1948**, *162*, 329–330.
(37) Russ, J. C.; Dehoff, R. T. *Practical Stereology*, 2nd ed.; Kluwer Academic/Plenum Publishers: New York, 2000.
(38) Daniels, H. E. *Proc. Cambridge Philos. Soc.* **1941**, *37*, 244–251.
(39) Kuhn, H. *Experientia* **1945**, *1*, 28–29.
(40) Kuhn, H. *Helv. Chim. Acta* **1948**, *31*, 1677–1690.
(41) Feller, W. *Ann. Math. Stat.* **1951**, *22*, 427–432.
(42) Weidmann, J. J.; Kuhn, H.; Kuhn, W. *J. Chim. Phys., Phys.-Chim. Biol.* **1953**, *50*, 226–235.
(43) Rubin, R. J. *J. Chem. Phys.* **1972**, *56*, 5747–5757.
(44) Mazur, J.; Rubin, R. J. *J. Chem. Phys.* **1974**, *60*, 341–342.
(45) Rubin, R. J.; Mazur, J. *J. Chem. Phys.* **1975**, *56*, 5362–5374.
(46) Rubin, R. J.; Mazur, J.; Weiss, G. H. *Pure Appl. Chem.* **1976**, *46*, 143–148.
(47) Rubin, R. J.; Weiss, G. H. *Macromolecules* **1977**, *10*, 332–334.
(48) Rubin, R. J.; Mazur, J. *Macromolecules* **1977**, *10*, 139–149.
(49) Weiss, G. H.; Rubin, R. J. *Adv. Chem. Phys.* **1983**, *52*, 363–505.
(50) de Gennes, P. G. *Scaling Concepts in Polymer Physics*; Cornell University Press: Ithaca, NY, 1979.
(51) Fleer, G. J.; Skvortsov, A. M. *Macromolecules* **2005**, *38*, 2492–2505.
(52) Clark, A. T.; Lal, M. *J. Chem. Soc., Faraday Trans.* **1981**, *2*, 981–996.
(53) Davidson, M. G.; Suter, U. W.; Deen, W. M. *Macromolecules* **1987**, *20*, 1141–1146.
(54) Cifra, P.; Bleha, T.; Romanov, A. *Polymer* **1988**, *29*, 1664–1668.
(55) Yethiraj, A.; Hall, C. K. *Mol. Phys.* **1991**, *73*, 503–515.
(56) Boyd, R. H.; Chance, R. R.; Ver Strate, G. *Macromolecules* **1996**, *29*, 1182–1190.
(57) Wang, Y.; Teraoka, I. *Macromolecules* **1997**, *30*, 8473–8477.
(58) Teraoka, I.; Cifra, P.; Wang, Y. *Macromolecules* **2001**, *34*, 7121–7126.
(59) Cifra, P.; Bleha, T. *Macromolecules* **2001**, *34*, 605–613.
(60) Chen, Z.; Escobedo, F. A. *Macromolecules* **2001**, *34*, 8802–8810.
(61) Cifra, P.; Teraoka, I. *Macromolecules* **2003**, *36*, 9638–9646.
(62) Cifra, P. *Macromolecules* **2005**, *38*, 3984–3989.
(63) Gong, Y.; Wang, Y. *Macromolecules* **2002**, *35*, 7492–7498.
(64) Jiang, W.; Khan, S.; Wang, Y. *Macromolecules* **2005**, *38*, 7514–7520.
(65) It is easy to prove that $C_2 \geq 0$ for any shaped objects since the second moment of $\max_i(x_i)$ is the same as that of $\max_i(y_i)$, and the latter variable is always lager than γ_{com}.We also speculate that the upper limit of C_2 is 1, but we have not found a proof for it. For a linear ideal chain, we found $C_2 \approx 0.8$ by fitting Casassa solution (eq 3 in ref 12) to eq 22 for the range of $0.01 \leq \lambda \leq 0.1$. Exact value may be obtained by expanding Casassa's solution to the second order at $\lambda \rightarrow 0$.
(66) Daoud, M.; de Gennes, P. G. *J. Phys.* (*Paris*) **1977**, *38*, 85–93.
(67) Grosberg, A. Y.; Khokhlov, A. R. *Statistical Physics of Macromolecules*; American Institute of Physics: New York, 1994.
(68) Cacciuto, A.; Luijten, E. *Nano Lett.* **2006**, *6*, 901–905.
(69) Sakaue, T.; Raphaël, E. *Macromolecules* **2006**, *39*, 2621–2628.
(70) Jun, S.; Arnold, A.; Ha, B.-Y. *Phys. Rev. Lett.* **2007**, *98*, 128303.
(71) Kennedy, T. *J. Stat. Phys.* **2002**, *106*, 407–429.

(72) Teraoka, I.; Langley, K. H.; Karasz, F. E. *Macromolecules* **1992**, *25*, 6106–6112.
(73) Rubinstein, M.; Colby, R. *Polymer Physics*; Oxford University Press: New York, 2003.
(74) Dubin, P. L.; Principi, J. M. *Macromolecules* **1989**, *22*, 1891–1896.
(75) Dünweg, B.; Reith, D.; Steinhauser, M.; Kremer, K. *J. Chem. Phys.* **2002**, *117*, 914–924.
(76) Douglas, J. F.; Roovers, J.; Freed, K. F. *Macromolecules* **1990**, *23*, 4168–4180.
(77) Hadjichristidis, N.; et al. *Macromolecules* **2000**, *33*, 2424–2436.
(78) Graessley, W. W. *Polymeric Liquids and Networks: Structure and Properties*; Taylor & Francis: New York, 2004.
(79) We would also like to address an additional feature in Figure 5, i.e., for branched chains of different architectures but the same g, it appears that both R_s/R_g and R_s/R_H are the largest for the symmetric star architecture; the values for other branched types are between those of linear and symmetric star architectures. It will be interesting to explore the universality of this finding.
(80) Tobita, H.; Saito, S. *Macromol. Theory Simul.* **1999**, *8*, 513–519.
(81) Tobita, H.; Hamashima, N. *Macromol. Theory Simul.* **2000**, *9*, 453–462.
(82) Tobita, H.; Hamashima, N. *J. Polym. Sci., Polym. Phys.* **2000**, *38*, 2009–2018.